Published as: Physical Review B 68, 054504 (2003) [doi:10.1103/PhysRevB.68.054504]

Shot noise in normal metal—d-wave superconducting junctions

Tomas Löfwander,[1] Mikael Fogelström,[1,2] and J. A. Sauls[1,*]

[1]Department of Physics & Astronomy, Northwestern University, Evanston, IL 60208
[2]Department of Theoretical Physics, Chalmers University of Technology and Göteborg University, S-412 96 Göteborg, Sweden

(Dated: April 25, 2003)

We present theoretical calculations and predictions for the shot noise in voltage biased junctions of $d_{x^2-y^2}$ superconductors and normal metal counter-electrodes. In the clean limit for the d-wave superconductor the shot noise vanishes at zero voltage because of resonant Andreev reflection by zero-energy surface bound states. We examine the sensitivity of this resonance to impurity scattering. We report theoretical results for the magnetic field dependence of the shot noise, as well the fingerprints of subdominant s- and d_{xy} pairing channels.

PACS numbers: 74.45.+c,74.40.+k,74.72.-h,74.50.+r

I. INTRODUCTION

It is now widely accepted that the order parameter in the superconducting state of the cuprates has $d_{x^2-y^2}$ symmetry. Several experiments, including the tri-crystal ring experiments,[1] corner junction experiments,[2] and the c-axis STM probes of impurity states,[3–5] have all provided strong evidence for the broken reflection symmetry of the $d_{x^2-y^2}$ order parameter.

Experiments based on tunnelling within the ab-plane are another class of experiments which provide valuable information about the properties of the cuprates. Conductance measurements on planar or point contact (by STM) normal metal—high-T_c superconducting junctions, and on Josephson junctions (e.g. grain boundaries) probe the electronic states of the cuprates near the surface or at the interface. In addition to changes in the atomic-scale structure of the interface, the $d_{x^2-y^2}$ superconducting state is highly distorted by interface scattering and disorder. The electronic spectrum is strongly modified, and the $d_{x^2-y^2}$ order parameter is in general suppressed on the coherence length scale. In fact, a standard feature of the ab-plane conductance is a large zero-bias conductance peak (ZBCP).[6–8] Its sensitivity to impurity scattering and the splitting of the peak in a magnetic field agree well with theoretical predictions[9–11] of surface Andreev bound states with large spectral weight that provide a resonant channel for tunnelling near zero bias. Normal scattering of quasiparticles by the surface from a positive lobe of the $d_{x^2-y^2}$ order parameter to a negative lobe, combined with Andreev reflection by the sudden π phase shift (sign change), leads to a zero-energy bound state.[12–14] In the case of a specular [110] surface all trajectories for quasiparticles are associated with a sign change of the order parameter, and thus the spectral weight of the Andreev states is very large.

In this paper we investigate theoretically the charge current through voltage-biased normal metal–insulating-barrier–d-wave superconductor (NIS) junctions subject to an external magnetic field directed along the c-axis. We extend the theory for the current fluctuations of conventional NIS junctions by Khlus[15] to voltage-biased NIS junctions with unconventional pairing correlations, as well as the effects field-induced surface currents on the current fluctuations. We present calculations of both the mean charge current and the charge current fluctuations, which at zero temperature reduce to the shot noise. We show that the resonant nature of Andreev reflection via the surface bound states in a clean $d_{x^2-y^2}$ superconductor can be used to extract additional information from the shot noise that cannot be obtained from conductance measurements alone. We discuss how the surface Andreev bound states (ABS) are broadened by impurity scattering. The impurity effect is reflected both in the conductance, which is related to the local density of states at the interface, and the shot noise, which reduces to $S = 2eI$ when impurity scattering dominates the intrinsic width of the surface ABS.

There are theoretical reasons to expect an additional, subdominant pairing state, e.g. with s- or d_{xy} symmetry, to be present in equilibrium under favorable circumstances.[9,16–19] The formation of surface states at the Fermi level, in combination with an attractive, subdominant pairing interaction favors a mixed-symmetry order parameter, e.g. a surface phase with $d_{x^2-y^2} \pm is$ or $d_{x^2-y^2} \pm id_{xy}$ symmetry. The sub-dominant component is predicted to have a phase of $\pm\pi/2$ relative to the dominant $d_{x^2-y^2}$ component, and thus to exhibit spontaneously broken time-reversal symmetry (T-symmetry). The internal phase of the order parameter leads to a shift of the bound state energies below the Fermi level, thus lowering the surface free energy and generating a spontaneous surface current.[9,17]

The splitting of the Andreev states also leads to the prediction that the ZBCP should spontaneously split as a function of voltage.[9] Such a splitting has been observed in YBCO near optimal doping.[6,20] However, in contrast to the general consensus about the $d_{x^2-y^2}$ pairing symmetry for the bulk phase of the cuprates, the nature of the surface phase, including the possibility of broken T-symmetry, is unsettled.[10,21] In the following we also discuss the "fingerprints" of sub-dominant pairing that may

be observable in the shot noise.

The theory of shot noise in mesoscopic, metallic systems has been used in several recent experiments to gain information about tunnelling in mesoscopic systems, see e.g. the recent review in Ref. 22. Earlier predictions for shot noise in d-wave NIS junctions were published by Zhu and Ting.[23] It was shown in a non-self-consistent calculation that for a clean d-wave superconductor the Andreev resonance associated with the surface Andreev bound states suppressed the shot noise to zero. It was confirmed in Ref. 24 that this effect also holds when self-consistency of the order parameter is taken into account. Recent theoretical work on noise in d-wave SIS junctions addresses the effects of surface disorder, interface states and magnetic fields on multiple Andreev reflection in this system, which is an important mechanism for noise in voltage-biased Josephson junctions.[25,26]

Here we report a detailed study of the shot noise, and specifically address physical conditions that are likely present at an NIS interface. The shot noise is shown to be particularly sensitive to the spectrum of surface states and to disorder. We present results for the magnetic field dependence of the shot noise, and demonstrate the sensitivity of the results obtained for clean d-wave superconductors to changes in the low-energy electronic spectrum by equilibrium surface currents and impurity scattering. We focus on the [110] orientation of an NIS interface to the cuprate superconductor, since for this orientation the influence of the Andreev bound states is most pronounced.

In Section II we describe our model of the normal metal-unconventional superconductor contact, beginning with a brief review of the quasiclassical Green's function technique that we use to compute observables. We discuss the boundary conditions for the non-equilibrium propagators, coherence amplitudes and distribution functions, and express these boundary conditions in terms of generalized scattering amplitudes. Explicit solutions are used to obtain results for the transport current and spectral density for current noise under nonequilibrium steady-state conditions. In Section III we present the results for the shot noise in voltage-biased NIS junctions with d-wave pairing symmetry for junctions with disorder near the interface. We discuss the effects of magnetic fields and screening currents and surface phase transitions on the noise spectrum. Throughout the paper we use units for which $\hbar = k_B = 1$, and we choose the sign convention $e = -|e|$.

II. THEORY AND INTERFACE MODEL

To compute the average current and fluctuations of the current we use the quasiclassical Green's function method,[27,28] and the Keldysh formalism to calculate non-equilibrium properties. The relevant information about the spectrum of current-carrying states and their distribution functions are contained in a set of non-equilibrium matrix Green's function: the retarded (R), advanced (A) and Keldysh (K) propagators, $\hat{g}^{R,A,K}(\mathbf{p}_f, \mathbf{R}; \epsilon, t)$, which are 4×4 matrix propagators in the combined spin and particle-hole space (Nambu space), that depend on the Fermi momentum, $\mathbf{p}_f$, the excitation energy, ϵ, and space and time coordinates, $\mathbf{R}$ and t. The quasiclassical propagators are related to the full Nambu propagators:

$$\begin{aligned}
\hat{G}^R(x,x') &= -i\Theta(t-t')\langle\{\Psi(x)\,,\,\bar{\Psi}(x')\}\rangle\,,\\
\hat{G}^A(x,x') &= +i\Theta(t'-t)\langle\{\Psi(x)\,,\,\bar{\Psi}(x')\}\rangle\,,\\
\hat{G}^K(x,x') &= -i\langle\big[\Psi(x)\,,\,\bar{\Psi}(x')\big]\rangle\,,
\end{aligned} \tag{1}$$

where the Nambu field operators, $\Psi(x) = (\psi_\uparrow(x), \psi_\downarrow(x), \psi^\dagger_\uparrow(x), \psi^\dagger_\downarrow(x))^{\rm tr}$, and $\bar{\Psi}(x) = \Psi^\dagger(x)$ incorporate particle-hole coherence of the superconducting state. We use the notation defined in Ref. 27 for the two-point functions where $\Theta(t)$ is the Heavyside function, $\{A, B\} = AB + BA$, and $[A, B] = AB - BA$. We also use the short-hand notation $x = (\mathbf{x}, t)$.

A compact formulation of the non-equilibrium equations is obtained in the Keldysh formulation in which the the set Nambu-matrix propagators, $\hat{G}^{R,A,K}$, are grouped into a 2×2 Keldysh matrix,

$$\check{G}(\mathbf{p}, \mathbf{R}; \epsilon, t) = \int dr\, e^{-i(\mathbf{p}\cdot\mathbf{r} - \epsilon\tau)} \begin{pmatrix} \hat{G}^R & \hat{G}^K \\ 0 & \hat{G}^A \end{pmatrix}. \tag{2}$$

It is most convenient to work in terms of the center-of-mass and relative coordinates, $R = (x + x')/2 = (\mathbf{R}, t)$ and $r = x - x' = (\mathbf{r}, \tau)$, and Fourier transform with the relative space and time coordinates. The quasiclassical propagators are then defined in terms of an integration of the full Keldysh-Nambu matrix propagator, $\check{G}(\mathbf{p}, \mathbf{R}; \epsilon, t)$, over an energy shell that is small compared with the Fermi energy, $|v_f(p - p_f)| < \varepsilon_c \ll E_f$,

$$\check{g}(\mathbf{p}_f, \epsilon; \mathbf{R}, t) = \frac{1}{a}\int_{-\varepsilon_c}^{+\varepsilon_c} d\xi_{\mathbf{p}}\, \check{\tau}_3 \check{G}(\mathbf{p}, \epsilon; \mathbf{R}, t)\,. \tag{3}$$

The quasiclassical propagator is defined by dividing out the weight of the quasiparticle pole in the spectral function, a, and by convention pre-multiplying by the matrix, $\check{\tau}_3 = \hat{\tau}_3\check{1}$. We denote a Nambu matrix with a 'hat', while Keldysh matrices are denoted with a 'check'. Thus, $\hat{\tau}_3$ is the third Pauli matrix in the particle-hole sector of Nambu space, and $\check{1}$ is the identity Keldysh matrix.

For pure spin-singlet pairing considered here the quasiclassical propagators, $\hat{g}^{R,A,K}$, may be parameterized in particle-hole space by scalar amplitudes for the diagonal (quasiparticle) and off-diagonal (Cooper pair) propagators,

$$\hat{g}^X = \begin{pmatrix} g^X & f^X \\ \underline{f}^X & \underline{g}^X \end{pmatrix}, \tag{4}$$

where $X = (R, A, K)$. We consider the case where the diamagnetic coupling of the charge currents to the magnetic field dominates the paramagnetic Zeeman coupling,

in which case the spin degrees of freedom are inert. The components of the quasiclassical propagators are then defined in terms of spin scalar diagonal propagators, g^X and $\underline{g}^X$, and spin-singlet off-diagonal propagators, f^X and $\underline{f}^X$. These components are not all independent, but are related by symmetries that follow from the fermion anti-commutation relations.[27]

For calculating the low-frequency ($\omega \ll \Delta, eV$) conductance and noise in NIS tunnel junctions we need only time-independent propagators. The steady-state nonequilibrium quasiclassical Keldysh-matrix propagator obeys a matrix transport equation,

$$[\epsilon\check{\tau}_3 - \check{v} - \check{\Sigma}\,,\, \check{g}] + i\mathbf{v}_f \cdot \boldsymbol{\nabla}\check{g} = 0\,, \tag{5}$$

where $\check{v} = e\Phi\check{1}$ is the electrostatic potential and $\check{\Sigma} = \check{\Delta} + \check{\Sigma}_{\rm imp}$ represents the order parameter and impurity self energy. The transport equation is supplemented by the normalization condition, $\check{g}^2 = -\pi^2\check{1}$,[29,30] and by boundary conditions connecting the propagators at the interface. When there is no reason for confusion, we do not display the dependence of $\check{g}$ and $\check{\Sigma}$ on $(\mathbf{p}_f, \mathbf{R}; \epsilon)$. Equation (5) represents coupled equations for the retarded, advanced,

$$\left[\hat{\rm H}^{R,A}\,,\, \hat{g}^{R,A}\right] + i\mathbf{v}_f \cdot \boldsymbol{\nabla}\hat{g}^{R,A} = 0\,, \tag{6}$$

and Keldysh propagators,

$$\begin{aligned}\hat{\rm H}^R\hat{g}^K - \hat{g}^K\hat{\rm H}^A \;&+\; \hat{g}^R\hat{\Sigma}^K - \hat{\Sigma}^K\hat{g}^A \\ &+\; i\mathbf{v}_f \cdot \boldsymbol{\nabla}\hat{g}^K = 0\,,\end{aligned} \tag{7}$$

where $\hat{\rm H}^{R,A} = \epsilon\hat{\tau}_3 - \hat{v} - \hat{\Sigma}^{R,A}$ is defined in terms of the excitation energy, ϵ, the coupling to external fields, $\hat{v}$, and the self-energies, $\hat{\Sigma}^{R,A}$. Similarly, the normalization condition expands to

$$\hat{g}^{R,A}\,\hat{g}^{R,A} = -\pi^2\,\hat{1}\,, \quad \hat{g}^R\,\hat{g}^K - \hat{g}^K\,\hat{g}^A = 0\,. \tag{8}$$

The retarded and advanced functions determine the particle-hole coherence functions and spectral properties at the NIS interface, while the Keldysh function contains additional information on the non-equilibrium distribution of these states.

The computation of $\check{g}$ involves solving the quasiclassical transport equations for the normal metal-insulating barrier-superconductor system together with a set of self-consistency equations for the impurity and pairing self-energies and boundary conditions in the bulk reservoirs and at the interface.

A. Pairing Model

The pairing correlations are described by the pairing self-energy, $\check{\Delta}$. In the leading order (weak-coupling) approximation, the Keldysh component vanishes and the retarded and advanced self-energies are independent of energy. The resulting self-consistency condition is the BCS gap equation,

$$\hat{\Delta}(\mathbf{p}_f, \mathbf{R}) = \left\langle \lambda(\mathbf{p}_f, \mathbf{p}'_f) \int_{-\epsilon_c}^{+\epsilon_c} \frac{d\epsilon}{4\pi i}\hat{f}^K(\mathbf{p}'_f, \mathbf{R}; \epsilon)\right\rangle_{\mathbf{p}'_f}. \tag{9}$$

where $\hat{f}^K(\mathbf{p}_f, \mathbf{R}; \epsilon)$ is the off-diagonal quasiclassical Keldysh propagator. We consider spin-singlet superconductivity derived from a pairing interaction of the form,

$$\lambda(\mathbf{p}_f, \mathbf{p}'_f) = \sum_\alpha \lambda_\alpha \eta_\alpha(\mathbf{p}_f)\eta_\alpha(\mathbf{p}'_f)\,, \tag{10}$$

where the sum is over the 'relevant' irreducible representations of the crystal point group, D_{4h}; $\alpha \in \{A_{1\rm g}(s-{\rm wave})B_{1\rm g}(d_{x^2-y^2}-{\rm wave}), B_{2\rm g}(d_{xy}-{\rm wave}), A_{2\rm g}(g-{\rm wave})\}$, and λ_α and $\eta_\alpha(\mathbf{p}_f)$ are the corresponding eigenvalues and eigenfunctions for pairing in channel α. The 'relevant' channels are defined by the dominant attractive eigenvalues for each irreducible representation obtained from solutions of the linearized gap equation with the microscopic pairing interaction (c.f. Ref. 19). The mechanism for pairing in the cuprates is not a solved problem, and indeed there may be more than one mechanism at work in the cuprates account for the wide range of superconducting properties as a function of doping and disorder. For example, a relatively simple two-channel model based on electronic coupling to anti-ferromagnetically correlated spin-excitations and to phonons leads to dominant $d_{x^2-y^2}$ pairing over a wide range of doping, but with significant sub-dominant pairing interactions in all other symmetry channels.[10] These sub-dominant pairing channels are predicted to play an important role in the local electronic structure of surface superconducting state near an insulating barrier or other interface.[19,31]

In this paper we consider the signatures of sub-dominant pairing in the shot noise. For this purpose we assume the dominant pairing channel has $d_{x^2-y^2}$ symmetry, and consider sub-dominant pairing in the s- or d_{xy} pairing channels, i.e. $\lambda_{B_{1g}} > \lambda_{B_{2g}}\ \lambda_{A_{1g}}$. The A_{2g} channel may also have an attractive eigenvalue for spin-fluctuation dominant pairing, but this order parameter is suppressed on both [110] and [100] boundaries, and is particularly sensitive to surface disorder, so we do not consider this sub-dominant channel for NIS junctions.

Below the superconducting transition temperature, T_c, the order parameter amplitude is proportional to the B_{1g} basis function, $\eta_{B_{1g}} = \sqrt{2}(\hat{p}_x^2 - \hat{p}_y^2)$. However, even a small attractive sub-dominant eigenvalue, $\lambda_{B_{2g}}$ or $\lambda_{A_{1g}}$ can, at low temperature generate a transition to a state with a mixed symmetry, with and order parameter that acquires an additional component proportional to the corresponding eigenfunction, $\eta_{B_{2g}} = \sqrt{2}\hat{p}_x\hat{p}_y$ or $\eta_{A_{1g}} = 1$.[53] Thus, in general we write the order parameter as

$$\Delta(\mathbf{p}_f, \mathbf{R}) = \sum_\alpha \Delta_\alpha(\mathbf{R})\eta_\alpha(\mathbf{p}_f)\,. \tag{11}$$

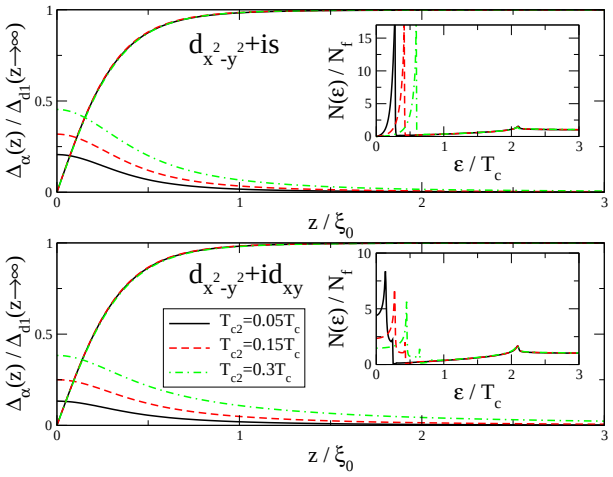

FIG. 1: Mixed-symmetry order parameters at a [110] specular surface. The relative phase between the $d_{x^2-y^2}$ and subdominant d_{xy} or s components is $\pm\pi/2$. The insets show the surface bound state spectrum for these mixed-symmetry phases. The calculations were carried out in the clean limit with $\Gamma = 0.001T_c$ and $\sigma = 10^{-4}$ (see text).

The gap equation separates into three self-consistency equations for each relevant pairing channel,

$$\Delta_\alpha(\mathbf{R}) = \lambda_\alpha \Big\langle \eta_\alpha(\mathbf{p}_f) \int_{-\epsilon_c}^{\epsilon_c} \frac{d\epsilon}{4\pi i} f^K(\mathbf{p}_f, \mathbf{R}; \epsilon) \Big\rangle_{\mathbf{p}_f} , \quad (12)$$

The solution of the transport equation and boundary conditions lead to coupling between the components, $\Delta_\alpha(\mathbf{R})$. The cutoff ϵ_c and pairing interaction, λ_α, are eliminated in favor of the instability temperatures, $T_{c\alpha}$, using the solution of the linearized gap equation, $\lambda_\alpha^{-1} = \ln(T/T_{c\alpha}) + \int (d\epsilon/2\epsilon) \tanh(\epsilon/2T)$. The overall phase of the order parameter (11) can be eliminated for an NIS system, but the relative phases between the different components that remain are determined by the minimum of the free energy. At sufficiently low temperature, the lowest energy state near a [110] surface is always a mixed symmetry phase with spontaneously broken T symmetry, in which the sub-dominant order parameter acquires a finite value with a relative phase of $\pm\pi/2$.[9,17] Consequently, we consider three possible order parameters: 1) pure $d_{x^2-y^2}$, 2) $d_{x^2-y^2} + is$, and 3) $d_{x^2-y^2} + id_{xy}$. Cases 2 and 3 are illustrated in Fig. (1), where the pairing interaction parameters are chosen so that the order parameter in the bulk region is always pure $d_{x^2-y^2}$, and the subdominant components are stable near the surface within a layer of the order of a few coherence lengths.

B. Magnetic Field and Screening Currents

One of the key features of the ABS interpretation of the zero-bias conductance peaks observed in ab-plane tunnelling spectroscopy is the splitting of the ZBCP for low magnetic fields.[8,20,32] The energy of the ABS is shifted away from the Fermi level by screening currents. The origin of this effect is the coupling of the quasiparticle current to the superflow field generated in response to the magnetic field,

$$\check{v}_{\rm A} = \mathbf{v}_f \cdot \mathbf{p}_s \check{\tau}_3 , \quad (13)$$

where the condensate flow field is given by the gauge-invariant gradient of the phase, $\mathbf{p}_s = \frac{1}{2}(\boldsymbol{\nabla}\vartheta - \frac{e}{c}\mathbf{A})$, where $\mathbf{A}$ is the vector potential. We include this coupling here in order to investigate the sensitivity of the noise spectrum to the spectral shift of the surface ABS. Indeed as we show below the shot noise is particularly sensitive to the Doppler shift of the zero energy surface states.

The condensate flow field, $\mathbf{p}_s$, is calculated by solving Maxwell's equation, self-consistently with the surface current, supplemented with the boundary conditions for magnetic field, $B \to 0$ for the Meissner state far from the surface, and $B \to H_{\rm ext}$ at the surface. For strong type II superconductors, such as the cuprates, with a magnetic penetration length $\lambda \gg \xi_0$, the solution of Maxwell's equation to leading order in the small parameter ξ_0/λ is $p_s(z) = p_{s0}e^{-z/\lambda}$ with

$$\frac{p_{s0}v_f}{T_c} = \frac{H_{\rm ext}}{H_0} - \frac{1}{\lambda}\int_0^\infty dz\, j_p(z) , \quad (14)$$

where $j_p(z)$ is the paramagnetic part of the current flowing parallel to the interface [computed via Eq. (31) below]. The paramagnetic current originates from the Doppler splitting of the ABS, which preferentially favors the paramagnetic response from the bound states.[9] The field scale in Eq. (14) is $H_0 = \Phi_0/(\pi\xi_0\lambda)$, where $\Phi_0 = c/2|e|$ is the flux quantum.

C. Impurity self energy

The anisotropic order parameter (Eq. 11) is sensitive to disorder. We include the leading order (in $1/p_f\ell_{\rm imp}$ where $\ell_{\rm imp}$ is the mean free path) effects of disorder within the model of isotropic scattering of quasiparticles by impurities (c.f. Ref. 33). In this model the impurity self-energy is given by the quasiparticle-impurity t-matrix and the average impurity concentration, $n_{\rm imp}$,

$$\check{\Sigma}_{\rm imp}(\mathbf{p}_f, \mathbf{R}; \epsilon) = n_{\rm imp}\check{t}(\mathbf{p}_f, \mathbf{p}_f, \mathbf{R}; \epsilon) , \quad (15)$$

where $\check{t}(\mathbf{p}_f, \mathbf{p}'_f, \mathbf{R}; \epsilon)$ satisfies a Bethe-Salpeter equation for repeated scattering of quasiparticles by impurities.[33] For isotropic impurity scattering defined by a scattering amplitude, u_0, the t-matrix equations for the retarded and advanced self-energies have the solutions,

$$\hat{t}^{R,A}(\mathbf{R}; \epsilon) = \frac{u_0\left[\hat{1} + u_0 N_f \langle \hat{g}^{R,A}(\mathbf{p}_f, \mathbf{R}; \epsilon)\rangle_{\mathbf{p}_f}\right]}{\hat{1} - \left[u_0 N_f \langle \hat{g}^{R,A}(\mathbf{p}_f, \mathbf{R}; \epsilon)\rangle_{\mathbf{p}_f}\right]^2} , \quad (16)$$

and the Keldysh component is given by

$$\hat{t}^K = N_f \hat{t}^R \langle \hat{g}^K \rangle_{\mathbf{p}_f} \hat{t}^A . \quad (17)$$

The scattering amplitude, u_0, defines the s-wave scattering phase shift, $\delta_0 = \arctan(\pi N_f u_0)$, while the impurity concentration and normal-state density of states define an energy scale $\Gamma_0 = n_{imp}/(\pi N_f)$. We use the more common parametrization of the impurity scattering model in terms of the dimensionless scattering cross section, $\sigma = \sin^2\delta_0$, and the pair breaking parameter, $\Gamma = \Gamma_0 \sin^2\delta_0$, or equivalently the mean-free path, $\ell_{\rm imp} = v_f/2\Gamma$.

The impurity self-energy renormalizes the excitation spectrum via, $\epsilon \to \tilde{\epsilon}(\mathbf{R}) = \epsilon - \Sigma_3^R(\epsilon, \mathbf{R})$, where Σ_3^R is the $\hat{\tau}_3$-component of $\hat{\Sigma}_{\rm imp}^R$. For a pure $d_{x^2-y^2}$ pairing state, the impurity renormalization of the order parameter vanishes by symmetry; the effects of pair-breaking are included through the renormalized excitation spectrum. As a result the solution of the gap equation shows a reduction of the order parameter amplitude with increasing pair breaking parameter, Γ. For mixed symmetry pairing, e.g. at the surface, and in the presence of field-induced screening currents, the pairing self-energy is, in general, non-vanishing and must be calculated self-consistently with the renormalization of the excitation spectrum.

In general the self-energy also includes electron correlation effects generated by electron-electron and electron-phonon interactions. In what follows we consider a simplified model for the metallic electrodes in which the quasiparticles are governed by an effective one-electron Hamiltonian with a parabolic band structure. Thus, the only electronic correlations included here are those that contribute to the effective mass, m^*, and give rise to superconductivity. In this case, $\mathbf{v}_f = \mathbf{p}_f/m^*$, and the charge current carried by a normal quasiparticle is $e\mathbf{v}_f = \frac{e}{m^*}\mathbf{p}_f$. Both the current and the noise spectrum are then calculated in this effective one-electron theory, modified to include pairing correlations in the superconductor, effects of screening currents on the surface excitation spectrum and impurity scattering in both electrodes.

D. Current and Current-Current Correlations

Physical properties, such as the local excitation spectrum, current response and correlation functions are expressed in terms of the quasiclassical Green's function. Here we are interested in computing the charge current and the mean-field fluctuations of the current for the NS junction. The junction current is an expectation value, in a nonequilibrium ensemble (ρ), of the Heisenberg operator for the charge current,

$$\begin{aligned}\mathsf{J}(\mathbf{r}_1, t_1) = \lim_{x_2\to x_1} \frac{-e}{2m^* i}\left(\nabla_1 - \nabla_2\right) \\ \left[\psi_\uparrow^\dagger(x_2)\psi_\uparrow(x_1) - \psi_\downarrow^\dagger(x_1)\psi_\downarrow(x_2)\right],\end{aligned} \tag{18}$$

Fluctuations of the current are related to the current-current correlation function, which is defined in terms of the operator,

$$\mathsf{S}(\mathbf{r}, t, \tau) \equiv \mathsf{K}(\mathbf{r}, t, t+\tau) + \mathsf{K}(\mathbf{r}, t+\tau, t)\,, \tag{19}$$

$$\begin{aligned}\mathsf{K}(\mathbf{r}_1, t_1, \tilde{t}_1) = \left(\frac{e}{2m^* i}\right)^2 \lim_{\tilde{\mathbf{r}}_1\to\mathbf{r}_1} \lim_{\substack{x_2\to x_1 \\ \tilde{x}_2\to\tilde{x}_1}} \left(\nabla_1 - \nabla_2\right)\left(\tilde{\nabla}_1 - \tilde{\nabla}_2\right) \\ \left[\psi_\uparrow^\dagger(x_2)\psi_\uparrow(x_1) - \psi_\downarrow^\dagger(x_1)\psi_\downarrow(x_2)\right]\left[\psi_\uparrow^\dagger(\tilde{x}_2)\psi_\uparrow(\tilde{x}_1) - \psi_\downarrow^\dagger(\tilde{x}_1)\psi_\downarrow(\tilde{x}_2)\right] - \mathbf{j}(\mathbf{r}_1, t_1)\mathbf{j}(\mathbf{r}_1, \tilde{t}_1)\,,\end{aligned} \tag{20}$$

where $\mathbf{j} = \mathrm{Tr}[\rho\,\mathsf{J}]$ is the expectation value of current operator. The observable noise is found by evaluating the average of this operator over the statistical ensemble, which is in general described by a nonequilibrium density matrix.

In what follows we consider the effects of scattering by point impurities (s-wave) in the superconducting electrode with d-wave pairing. For the steady-state conductance and current noise the statistical average for the noise reduces to the product of two-point correlation functions. Vertex corrections to the current-current correlator vanish in the above approximations, or originate from quantum interference effects or coupling to collective modes and thus are higher order in $1/p_f\ell_{\rm imp}$ or $1/p_f\xi_0$, and neglected here. Thus, after integration over the cross section of the junction, $\mathcal{A}$, we obtain the current noise, $S(z_1, t_1, \tilde{t}_1)$,

$$S = \frac{1}{2}\left(\frac{e}{2m^* i}\right)^2 \lim_{\substack{\mathbf{r}_2\to\mathbf{r}_1 \\ \tilde{\mathbf{r}}_2\to\tilde{\mathbf{r}}_1 \\ \tilde{\mathbf{r}}_1\to\mathbf{r}_1}} \int d^2 r_{1\parallel} \int d^2\tilde{r}_{1\parallel} \left(\partial_{z_1} - \partial_{z_2}\right)\left(\partial_{\tilde{z}_1} - \partial_{\tilde{z}_2}\right) \mathrm{Tr}\left\{\hat{G}^<(\tilde{\mathbf{r}}_1, \mathbf{r}_2; \tilde{t}_1, t_1)\hat{G}^>(\mathbf{r}_1, \tilde{\mathbf{r}}_2; t_1, \tilde{t}_1)\right\}, \tag{21}$$

where $\hat{G}^{\gtrless} = \hat{G}^K \pm (\hat{G}^R - \hat{G}^A)$ are the particle ($<$) and hole ($>$) correlation functions.

We separate out the momentum component parallel to the junction using the inverse Fourier transformation with respect to the difference coordinate $\mathbf{r}_\parallel = \mathbf{r}_{1\parallel} - \mathbf{r}_{2\parallel}$,

$$\check{G}(\mathbf{r}_1, \mathbf{r}_2) = \int \frac{d^2 p_\parallel}{(2\pi)^2} e^{i\mathbf{p}_\parallel \cdot \mathbf{r}_\parallel} \check{G}(z_1, z_2, \mathbf{p}_\parallel, \mathbf{R}_\parallel)\,, \qquad (22)$$

and assume that the dependence on $\mathbf{R}_\parallel$ is slow on the scale of the coherence length, i.e. locally planar; thus, we omit $\mathbf{R}_\parallel$. Near the junction, incident and scattered waves interfere on a scale given by the inverse Fermi momentum p_f^{-1}. We then make the following *ansatz*,[15,34,35] which factors the propagator into rapidly oscillating incident and reflected waves with wavenumbers, $\pm p_{fz}$, and slowly varying two-point envelope functions,

$$\check{\tau}_3 \check{G}(z_1, z_2) = \frac{1}{v_{fz}} \sum_{\nu\mu} \check{C}_{\nu\mu}(z_1, z_2) e^{ip_{fz}(\nu z_1 - \mu z_2)}\,, \qquad (23)$$

where z is the coordinate normal to the interface. The sum is over *direction* indices ν and μ which are $+1$ or -1, depending on the sign of the projection of the Fermi momentum on the z-axis for incident or reflected waves (see Fig. 2). When ν appears as an index of a function we use a shorthand notation $\pm$ for ± 1. The diagonal (in direction index space) functions $\check{C}_{\nu\nu}$ are related to Shelankov's two-point quasiclassical Green's functions.[36] In the limits, $z_2 \to z_1 \pm 0$, these components are related to the projection operators,

$$\mp i \underset{--}{\overset{++}{\check{C}}} = \check{P}_\mp = \frac{1}{2}\left(\check{1} \mp \frac{\check{g}}{-i\pi}\right). \qquad (24)$$

The functions $\check{C}_{\nu(-\nu)}$ are the pre-factors of the rapidly oscillating carrier waves, $\sim e^{\pm 2ip_{fz}z}$. These amplitudes are *drones* - slaved to the quasiclassical propagators and ultimately eliminated from the boundary conditions and observables such as the current noise. In particular, Zaitsev's boundary conditions[34] are derived (for details see Ref. 35) by eliminating the drone amplitudes from a set of linear relations connecting the quasiclassical projectors, $\check{C}_{\nu\nu}$ and the quasiclassical drones, $\check{C}_{\nu(-\nu)}$. This procedure transforms the linear boundary conditions expressed in terms of the set, $\{\check{C}_{\nu\mu}\}$, into a set of non-linear boundary conditions for the quasiclassical projectors, $\check{C}_{\nu\nu}$, and consequently for the quasiclassical Green's functions.

For the average current, the expectation value of the operator in Eq. 18 can be expressed as

$$I(z_1, t_1) = \frac{e}{8m^*} \int d^2 r_{1\parallel} \lim_{x_2 \to x_1} (\partial_{z1} - \partial_{z2}) \\ \mathrm{Tr}\left\{\hat{G}^K(x_1, x_2) - \hat{\tau}_3\left[\hat{G}^R(x_1, x_2) - \hat{G}^A(x_1, x_2)\right]\right\}, \qquad (25)$$

for the current flowing through the junction along the z-axis. When we insert the quasiclassical envelope expansions, Eqs. (22)-(23), the derivatives produce a factor $ip_{fz}(\nu + \mu) = 2ip_{fz}\delta_{\nu\mu}$, and the current takes the form

$$I(z_1, t) = \mathcal{A}\frac{ie}{2} \lim_{z_2 \to z_1} \int \frac{d^2 p_\parallel}{(2\pi)^2} \int \frac{d\epsilon}{2\pi} \sum_\nu \nu \times \\ \mathrm{Tr}\left\{\tau_3 \hat{C}^K_{\nu\nu}(z_1, z_2, \mathbf{p}_\parallel; \epsilon, t)\right\}, \qquad (26)$$

where we neglect terms where the derivative act on quasiclassical Green's functions since they are down by a factor $(p_f \xi_0)^{-1}$ compared to the leading term above. Also note that the term $\hat{C}^R - \hat{C}^A$ drops out because spectral current density is odd in energy to this order in $(p_f\xi_0)^{-1}$.

When we insert the quasiclassical expressions, Eqs. (22)-(23), into the expression for the noise, Eq. (21), the derivatives produce a factor $(ip_{fz})^2(\tilde{\nu} + \mu)(\nu + \tilde{\mu}) = (2ip_{fz})^2 \delta_{\tilde{\nu}\mu}\delta_{\tilde{\mu}\nu}$, where the indices without (with) a tilde belong to the first (second) Green's function. Thus, to quasiclassical accuracy we obtain,

$$S(z_1, t_1, \tilde{t}_1) = \mathcal{A}\frac{e^2}{2} \lim_{\tilde{z}_1 \to z_1} \int \frac{d^2 p_\parallel}{(2\pi)^2} \sum_{\nu\mu} \nu\mu \times \qquad (27) \\ \mathrm{Tr}\{\hat{C}^<_{\nu\mu}(\tilde{z}_1, z_1, \mathbf{p}_\parallel; \tilde{t}_1, t_1)\hat{\tau}_3 \hat{C}^>_{\mu\nu}(z_1, \tilde{z}_1, \mathbf{p}_\parallel; t_1, \tilde{t}_1)\hat{\tau}_3\}\,,$$

where $\mathcal{A}$ is the cross-sectional area of the junction - which is the result previously obtained by Khlus[37] for conventional NS junctions.

The spectral density of the noise is given by the Fourier transform,[22] $S(z, t, \omega) = \int dt e^{i\omega\tau} S(z, t, \tau)$, which for general non-equilibrium conditions depends on time. Here we consider the d.c. limit for the voltage-biased junction. This steady-state limit is independent of time, so we drop the time argument from here on.

The drones, as well as the quasiclassical correlation functions, $\hat{C}^{\gtrless}_{\nu\nu}(\tilde{z}_1, z_1) = \hat{C}^K \pm (\hat{C}^R - \hat{C}^A)$, are continuous and single-valued for $\tilde{z}_1 = z_1$.[35] Thus, we may take the limit $\tilde{z}_1 \to z_1$; the diagonal functions are proportional to the corresponding quasiclassical Green's functions,

$$\lim_{z_2 \to z_1} \hat{C}^{\gtrless}_{\nu\nu}(z_1, z_2) = \frac{\hat{g}^{\gtrless}_\nu(z_1)}{2\pi}\,, \qquad (28)$$

and we introduce the following notation for the drones,

$$\lim_{z_2 \to z_1} \hat{C}^{\gtrless}_{\nu(-\nu)}(z_1, z_2) = \frac{\hat{d}^{\gtrless}_{\nu(-\nu)}(z_1)}{2\pi}\,. \qquad (29)$$

Thus, the current is written as

$$I = -eN_f\mathcal{A} \int \frac{d\epsilon}{4\pi i} \sum_{\nu=\pm 1} \nu\ \mathrm{Tr}\left\langle v_{fz}\hat{\tau}_3 \hat{g}^K_\nu \right\rangle_\nu\,, \qquad (30)$$

which is the z-component of the more general quasiclassical result for the current density,

$$\mathbf{j} = -eN_f \int \frac{d\epsilon}{4\pi i} \mathrm{Tr}\left\langle \mathbf{v}_f \hat{\tau}_3 \hat{g}^K \right\rangle_{\mathbf{p}_f}\,, \qquad (31)$$

where N_f is the normal-state density of states at the Fermi level and $\langle \ldots \rangle_{\mathbf{p}_f} = N_f^{-1} \int \frac{d^2 p_f}{((2\pi)^3 |\mathbf{v}(\mathbf{p}_f)|}(\ldots)$ denotes a Fermi surface average.

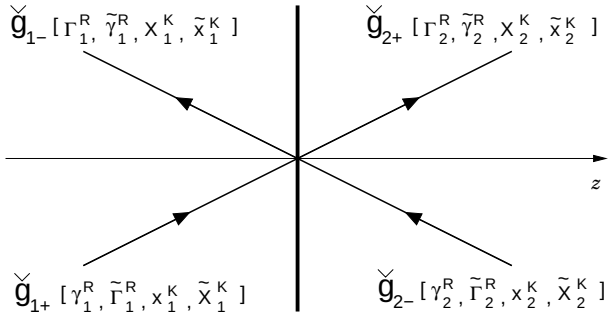

FIG. 2: We label Green's functions by an index 1 for the left (normal) electrode and 2 for the right (superconducting) electrode, and a direction index $\pm$ which denotes the sign of the projection of the Fermi momentum $\mathbf{p}_f$ on the z-axis. The arrows on each line indicates the direction of $\mathbf{p}_f$. Also shown is the notation for the propagators, coherence amplitudes and distribution functions.

Similarly, the local noise spectrum may be written as

$$S = e^2 N_f \mathcal{A} \int d\tau\, e^{i\omega\tau} \int \frac{d\epsilon}{16\pi^2} \sum_{\nu=\pm 1} \times \qquad (32)$$
$$\mathrm{Tr}\left\langle v_{fz}\left(\hat{g}^<_\nu \hat{\tau}_3 \hat{g}^>_\nu \hat{\tau}_3 - \hat{d}^<_{\nu(-\nu)}\hat{\tau}_3 \hat{d}^>_{(-\nu)\nu}\hat{\tau}_3\right)\right\rangle_\nu ,$$

where $\langle \ldots \rangle_\nu$ denotes a Fermi surface average restricted to $\mathrm{sgn}(\mathbf{p}_f \cdot \hat{z}) = \nu$. Although the noise formula in Eq. (32) depends on the drones, they do not require independent calculation from their equations of motion, but are expressed in terms of the quasiclassical propagators (see below).

E. Interface Boundary Conditions

In order to compute the transport current and noise spectrum we must solve transport equations for the quasiclassical propagators, and drones, with appropriate boundary conditions describing the junction. Quasiclassical boundary conditions describing partially transmitting interfaces between conducting electrodes were derived by Zaitsev[34] and Kieselmann[38] for non-magnetic junctions, and by Millis et al.[35] for magnetically active interfaces. Zaitsev and Kieselmann's boundary conditions are a set of nonlinear equations connecting the quasiclassical propagators for incoming and outgoing trajectories at the interface. The material parameters entering these boundary conditions are the reflection ($\mathcal{R}$) and transmission ($\mathcal{D} = 1 - \mathcal{R}$) probabilities for quasiparticles when both electrodes are in their normal-states. This formulation is valid for arbitrary transparency.

The quasiclassical boundary conditions, when one or both electrodes are superconducting, incorporate the effects of particle-hole coherence of the excitations in the superconducting electrodes, *and* the presence of additional channels for reflection and transmission via branch conversion scattering between particle- and hole-like branches of excitations.

A powerful method for handling the interplay between these coherence effects and interface scattering was provided by Eschrig's reduction[39] of Zaitsev and Kieselmann's boundary conditions using Schelankov's projection operators[36] and the Ricatti parametrization for the quasiclassical propagators.[40–42] The boundary condition is expressed in terms of coherence functions, γ^R and $\tilde{\gamma}^R$, and distribution functions, x^K and $\tilde{x}^K$. The coherence functions have a natural interpretation as local amplitudes for branch conversion; γ^R for $h \to e$ and $\tilde{\gamma}^R$ for $e \to h$. Below we express these boundary conditions in terms of generalized scattering amplitudes, which in the clean limit are directly related to well known scattering amplitudes found in scattering theory.[22] The considerations below are valid for general non-equilibrium situations, but the results presented below are limited to time-independent states. For non-stationary states, all multiplications are replaced by time-convolutions, which in general prevents analytic computations.

We adopt the notation used in Ref. 39 for the coherence amplitudes and distribution functions. The labelling for functions defined on incoming and outgoing trajectories is also indicated in Fig. 2. For the distribution functions, the boundary conditions can be written as

$$X_1^K = R^R_{ee} x_1^K + \bar{T}^R_{ee} x_2^K + (-\bar{T}^R_{eh})\tilde{x}_2^K, \qquad (33)$$
$$\tilde{X}_1^K = R^R_{hh} \tilde{x}_1^K + (-\bar{T}^R_{he}) x_2^K + \bar{T}^R_{hh}\tilde{x}_2^K, \qquad (34)$$
$$X_2^K = T^R_{ee} x_1^K + (-T^R_{eh})\tilde{x}_1^K + \bar{R}^R_{ee} x_2^K, \qquad (35)$$
$$\tilde{X}_2^K = (-T^R_{he}) x_1^K + T^R_{hh}\tilde{x}_1^K + \bar{R}^R_{hh}\tilde{x}_2^K, \qquad (36)$$

where the scattering amplitudes are defined as

$$r^R_{ee} = R^R_{1l}/r, \quad \bar{t}^R_{ee} = D^R_{1l}/d, \quad \bar{t}^R_{eh} = rdA^R_{1l}, \qquad (37)$$
$$r^R_{hh} = \tilde{R}^R_{1l}/r, \quad \bar{t}^R_{hh} = \tilde{D}^R_{1l}/d, \quad \bar{t}^R_{he} = rd\tilde{A}^R_{1l}, \qquad (38)$$
$$\bar{r}^R_{ee} = R^R_{2l}/r, \quad t^R_{ee} = D^R_{2l}/d, \quad t^R_{eh} = rdA^R_{2l}, \qquad (39)$$
$$\bar{r}^R_{hh} = \tilde{R}^R_{2l}/r, \quad t^R_{hh} = \tilde{D}^R_{2l}/d, \quad t^R_{he} = rd\tilde{A}^R_{2l}\,. \qquad (40)$$

The right-hand sides of Eqs. (37-40) are defined in Eqs. (D1-D5) of Ref. 39. Note that all quantities depend on trajectory angle $\mathbf{p}_f$ and energy ϵ, but not on spatial coordinates $\mathbf{R}$ since they are evaluated at the junction. The normal-state tunnel barrier transmission and reflection amplitudes are denoted d and r, respectively, while the corresponding probabilities are denoted by $\mathcal{D} = d^2$ and $\mathcal{R} = r^2$.[54]

The effective transmission and reflection amplitudes, including Andreev scattering, are denoted by $t^R_{\alpha\beta}$ and $r^R_{\alpha\beta}$, while the corresponding probabilities are denoted as $T^R_{\alpha\beta}$ and $R^R_{\alpha\beta}$. For example, r^R_{hh} is the amplitude for reflection of a hole on the left side of the junction, while $\bar{r}^R_{ee}$ is the amplitude for reflection of an electron on the right side. Similarly, $\bar{t}^R_{he}$ is the transmission amplitude for an electron from the right side to the left side, including

branch conversion into a hole. All quantities with a bar refer to excitations originating from the right electrode.

The remaining amplitudes are the Andreev reflections, which appear via the boundary conditions for the coherence functions,

$$r^R_{he} = \tilde{\Gamma}^R_1 = r^R_{hh}\tilde{\gamma}^R_1 r + \bar{t}^R_{hh}\tilde{\gamma}^R_2 d, \quad (41)$$
$$r^R_{eh} = \Gamma^R_1 = r^R_{ee}\gamma^R_1 r + \bar{t}^R_{ee}\gamma^R_2 d, \quad (42)$$
$$\bar{r}^R_{he} = \tilde{\Gamma}^R_2 = \bar{r}^R_{hh}\tilde{\gamma}^R_2 r + t^R_{hh}\tilde{\gamma}^R_1 d, \quad (43)$$
$$\bar{r}^R_{eh} = \Gamma^R_2 = \bar{r}^R_{ee}\gamma^R_2 r + t^R_{ee}\gamma^R_1 d\,. \quad (44)$$

In the Appendix we summarize the results for the Andreev reflection probabilities and scattering probabilities that enter the Keldysh distribution functions in Tables (II-III). These probabilities are expressed in terms of the normal-state barrier transmission and reflection probabilities, and the coherence amplitudes for particle and hole excitations.

We introduce the notation,

$$|\alpha\rangle = \begin{pmatrix} 1 \\ -i\sigma_y\alpha \end{pmatrix}, \qquad \langle\alpha| = (1,\ -i\sigma_y\alpha^*)\,, \quad (45)$$

which is convenient for evaluating observables. For example, to calculate the charge current we need

$$\mathrm{Tr}\,\{\hat{\tau}_3|\alpha\rangle\langle\beta|\} = 2(1+\alpha\beta^*)\,, \quad (46)$$

where the factor 2 comes from the spin trace. The Keldysh Green's functions at the junction can now be written in a rather compact form,

$$\begin{aligned}
\hat{g}^K_{1+} &= -2\pi i N_1^{-1}\left[x^K_1|r^R_{he}\rangle\langle r^R_{he}| + \tilde{X}^K_1\hat{\tau}_1|\gamma^R_1\rangle\langle\gamma^R_1|\hat{\tau}_1\right],\\
\hat{g}^K_{1-} &= -2\pi i N_2^{-1}\left[\tilde{x}^K_1\hat{\tau}_1|r^R_{eh}\rangle\langle r^R_{eh}|\hat{\tau}_1 + X^K_1|\tilde{\gamma}^R_1\rangle\langle\tilde{\gamma}^R_1|\right],\\
\hat{g}^K_{2-} &= -2\pi i N_3^{-1}\left[x^K_2|\bar{r}^R_{he}\rangle\langle\bar{r}^R_{he}| + \tilde{X}^K_2\hat{\tau}_1|\gamma^R_2\rangle\langle\gamma^R_2|\hat{\tau}_1\right],\\
\hat{g}^K_{2+} &= -2\pi i N_4^{-1}\left[\tilde{x}^K_2\hat{\tau}_1|\bar{r}^R_{eh}\rangle\langle\bar{r}^R_{eh}|\hat{\tau}_1 + X^K_2|\tilde{\gamma}^R_2\rangle\langle\tilde{\gamma}^R_2|\right],
\end{aligned} \quad (47)$$

where we introduced the denominators, $N_i = |\zeta_i|^2$ for $i = 1..4$ with

$$\zeta_1 = 1+\gamma^R_1 r^R_{he} \qquad \zeta_3 = 1+\gamma^R_2\bar{r}^R_{he}, \quad (48)$$
$$\zeta_2 = 1+\tilde{\gamma}^R_1 r^R_{eh} \qquad \zeta_4 = 1+\tilde{\gamma}^R_2\bar{r}^R_{eh}\,. \quad (49)$$

Note that all denominators of the scattering probabilities in Eqs. (33)-(36) (see Table III in the Appendix) are cancelled by the denominators, N_i, in Eqs. (47); e.g. $R^R_{ee}N_1^{-1} = (A/\zeta_1)*(\zeta_1/|Z|^2) = A/|Z|^2 = R^{R'}_{ee}$. As a consequence, a common denominator, $|Z|^2$, enters all Keldysh propagators,

$$\begin{aligned}
Z = 1 &+ R(\gamma^R_2\tilde{\gamma}^R_2 + \gamma^R_1\tilde{\gamma}^R_1)\\
&+ D(\gamma^R_2\tilde{\gamma}^R_1 + \tilde{\gamma}^R_2\gamma^R_1) + \gamma^R_1\tilde{\gamma}^R_1\gamma^R_2\tilde{\gamma}^R_2\,.
\end{aligned} \quad (50)$$

This function also appears as the denominator of the retarded Green's function. Thus, the zeroes of Z determine the local spectrum of excitations, including interface bound states, at the junction.

TABLE I: Scattering amplitudes at an NIS juntion. The common denominator is $Z = 1+\mathcal{R}\gamma^R\tilde{\gamma}^R$

$r^R_{ee} = \frac{r(1+\gamma^R\tilde{\gamma}^R)}{Z}$	$r^R_{hh} = \frac{r(1+\gamma^R\tilde{\gamma}^R)}{Z}$	$\bar{r}^R_{ee} = \frac{r}{Z}$	$\bar{r}^R_{hh} = \frac{r}{Z}$
$r^R_{he} = \frac{\mathcal{D}\tilde{\gamma}^R}{Z}$	$r^R_{eh} = \frac{\mathcal{D}\gamma^R}{Z}$	$\bar{r}^R_{he} = \mathcal{R}\tilde{\gamma}^R$	$\bar{r}^R_{eh} = \mathcal{R}\gamma^R$
$t^R_{ee} = \frac{d}{Z}$	$t^R_{hh} = \frac{d}{Z}$	$\bar{t}^R_{ee} = \frac{d}{Z}$	$\bar{t}^R_{hh} = \frac{d}{Z}$
$t^R_{he} = \frac{rd\tilde{\gamma}^R}{Z}$	$t^R_{eh} = \frac{rd\gamma^R}{Z}$	$\bar{t}^R_{he} = -\frac{rd\tilde{\gamma}^R}{Z}$	$\bar{t}^R_{eh} = -\frac{rd\gamma^R}{Z}$

We note that the scattering amplitudes defined above do not exactly coincide with the ones obtained in scattering theory. There are missing pre-factors, which are hidden in the matrices $|\alpha\rangle\langle\alpha|$ in Eqs. (47), and in the distribution functions x^K and $\tilde{x}^K$ [e.g. in equilibrium, $x^K = (1-|\gamma^R|^2)\tanh(\epsilon/2T)$]. Inspection shows that our generalized scattering amplitudes can be interpreted as describing the scattering of *locally* defined excitations at the junction, while the factors coming from the matrices and distribution functions gives a spectral renormalization due to Andreev reflection along the trajectories leading up to (and away from) the interface. For example, when a charge current is computed, these renormalizations can be absorbed into the scattering amplitudes, which then coincide with results from scattering theory. However, we retained the above definitions since they appear naturally in the boundary condition for Green's functions.

The above considerations are applicable to stationary states of two coupled superconductors driven out of equilibrium. For the special case in which the left electrode, is in the normal state, $\gamma^R_1 = \tilde{\gamma}^R_1 = 0$. Using Eq. (46) we obtain the current computed at the junction on the left side of the barrier

$$\begin{aligned}
I = eN_f\mathcal{A}\int d\epsilon\,\big\langle v_{fz}\big[&x^K_1(1+R^R_{he}-R^R_{ee})\\
&+\tilde{x}^K_1(1+R^R_{eh}-R^R_{hh})\\
&+x^K_2(\bar{T}^R_{he}-\bar{T}^R_{ee}) + \tilde{x}^K_2(\bar{T}^R_{eh}-\bar{T}^R_{hh})\big]\big\rangle_{\mathbf{p}_f}\,.
\end{aligned} \quad (51)$$

Explicit expressions for the effective scattering amplitudes are given in Table I for the NIS junction. Equation (51) is valid for arbitrary stationary non-equilibrium situations, including spatially dependent coherence and distribution functions. Current conservation is guaranteed for self-consistent calculations.

F. Asymptotic Boundary Conditions

In the reservoir regions, far from the junction, the distribution functions take the equilibrium forms, shifted by the local potential,

$$\begin{aligned}
F_1(x\to-\infty,\epsilon) &= \tanh[(\epsilon-eV)/(2T)],\\
F_2(x\to+\infty,\epsilon) &= \tanh[\epsilon/(2T)].
\end{aligned} \quad (52)$$

The hole distributions follow by symmetry $\tilde{F}(\epsilon) = F(-\epsilon)$. We neglect processes where quasiparticles scattered at the junction are scattered back and impinge on

the junction before they equilibrate. The above distribution functions then serve as incoming distribution functions in the boundary condition at the junction. We shall also assume that the transparency of the junction is sufficiently small, $\mathcal{D} \ll 1$, that the current flowing throught the system (which is proportional to $\mathcal{D}$) due to the applied voltage is small. Then, to lowest order in $\mathcal{D}$ we can neglect the effect of the current on the order parameter and write

$$f^K(\mathbf{p}_f, \mathbf{R}; \epsilon) = \left[f^R - f^A\right] \tanh \frac{\epsilon}{2T}\,, \tag{53}$$

which is the local equilibrium form for the off-diagonal Keldysh propagator. We note that these assumptions will be valid also for high-transparency point contacts and for wide junctions with transport primarily through a high-transparency pinhole, since the current in those cases are reduced by the small conducting area $A \ll \pi\xi_0^2$, where $\xi_0 = v_f/T_c$ is the superconducting coherence length.

Under these assumptions, the interface distribution functions are,

$$x_1^K = F_1\,, \qquad x_2^K = (1 - |\gamma^R|^2)F_2 \tag{54}$$

$$\tilde{x}_1^K = \tilde{F}_1\,, \qquad \tilde{x}_2^K = -(1 - |\tilde{\gamma}^R|^2)F_2 \quad , \tag{55}$$

where we drop the subscript 2 on coherence functions since they are superfluous for an NIS system. The x_2^K and $\tilde{x}_2^K$ terms then cancel in Eq. (51 by the general tilde-symmetry, which relates any quantity $\tilde{q}$ to its partner q as $\tilde{q}(\mathbf{p}_f, \mathbf{R}; \epsilon, t) = q(-\mathbf{p}_f, \mathbf{R}; -\epsilon, t)^*$. However, the x_1^K and $\tilde{x}_1^K$ terms are only equal at zero bias because particles and holes have opposite charge.

G. Drone Green's functions and noise

To compute the noise in Eq. (32) we need to also compute the drone amplitudes $\check{d}_{\nu(-\nu)}$. The relations connecting the drones to the quasiclassical propagators are the same equations used to obtain the nonlinear boundary condition connecting the quasiclassical propagators $\check{g}_{1\pm}$ and $\check{g}_{2\pm}$.[34,35] Thus, we define the symmetric combination of Green's functions on the two sides ($i = 1, 2$) of the interface as

$$\check{g}_{is} = \check{g}_{i+} - \check{g}_{i-}, \tag{56}$$

and symmetric and anti-symmetric combinations of drones as

$$\begin{aligned} \check{d}_{is} &= \check{d}_{i+-} + \check{d}_{i-+}, \\ \check{d}_{ia} &= \check{d}_{i+-} - \check{d}_{i-+}. \end{aligned} \tag{57}$$

The necessary relations are then

$$\begin{aligned} \check{d}_{1s} &= \frac{1}{2\sqrt{\mathcal{R}}}\left[(1+\mathcal{R})\check{g}_{1s} - \mathcal{D}\check{g}_{2s}\right], \\ \check{d}_{2s} &= \frac{1}{2\sqrt{\mathcal{R}}}\left[\mathcal{D}\check{g}_{1s} - (1+\mathcal{R})\check{g}_{2s}\right], \\ 4\pi i\check{d}_{1a} &= \check{g}_{1s}\check{d}_{1s} - \check{g}_{2s}\check{d}_{2s}, \end{aligned} \tag{58}$$

where the first two relations come from the boundary condition, and the last relation is derived by making use of the normalization condition for Green's functions [c.f. Eqs. (29)-(30) of Ref. 35]. We note that we are content with solving for the drones on the left side. Explicit expressions of the drones can then be written down by using the Green's function $\check{g}$ written in terms of scattering amplitudes in Table I. The retarded and advanced drones are

$$\hat{d}_{1s}^R = -2\pi i r_{ee}^R \hat{\tau}_3, \qquad \hat{d}_{1s}^A = +2\pi i r_{ee}^{R*}\hat{\tau}_3, \tag{59}$$

$$\hat{d}_{1a}^R = +2\pi i r_{ee}^R \hat{1}, \qquad \hat{d}_{1a}^A = +2\pi i r_{ee}^{R*}\hat{1}\,, \tag{60}$$

while Keldysh drones take the form

$$\begin{aligned} B &= x_1^K r_{ee}^R r_{he}^{R*} + \tilde{x}_1^K r_{hh}^{R*} r_{eh}^R - x_2^K \bar{t}_{ee}^R \bar{t}_{he}^{R*} - \tilde{x}_2^K \bar{t}_{hh}^{R*}\bar{t}_{eh}^R\,, \\ \hat{d}_{1s}^K &= -2\pi i \begin{pmatrix} x_1^K(r_{ee}^R + r_{ee}^{R*}) & -i\sigma_y B \\ -i\sigma_y B^* & \tilde{x}_1^K(r_{hh}^R + r_{hh}^{R*}) \end{pmatrix}, \\ \hat{d}_{1a}^K &= +2\pi i \begin{pmatrix} x_1^K(r_{ee}^R - r_{ee}^{R*}) & -i\sigma_y B \\ +i\sigma_y B^* & -\tilde{x}_1^K(r_{hh}^R - r_{hh}^{R*}) \end{pmatrix}. \end{aligned} \tag{61}$$

where $i\sigma_y$ is the Pauli matrix that describes spin-singlet pairing.

Since the noise is expressed in terms of $\hat{g}^{\gtrless} = \hat{g}^K \pm (\hat{g}^R - \hat{g}^A)$ and $\hat{d}^{\gtrless} = \hat{d}^K \pm (\hat{d}^R - \hat{d}^A)$, we get terms from the Keldysh parts which depend explicitly on the distribution functions, and purely spectral terms that do not contain any distribution functions. Thus, we separate the noise into two terms, $S = S^{R-A} + S^K$, where

$$\begin{aligned} S^{R-A}(\mathbf{p}_f, x = 0^-; \epsilon) = 4\big[&(1 + R_{he}^R - R_{ee}^R) + \\ &(1 + R_{eh}^R - R_{hh}^R)\big]\,, \end{aligned} \tag{62}$$

$$
\begin{aligned}
S^K(\mathbf{p}_f, x=0^-;\epsilon) = &-(x_1^K)^2 2\left[1+R_{he}^R-R_{ee}^R\right]^2 - (\tilde{x}_1^K)^2 2\left[1+R_{eh}^R-R_{hh}^R\right]^2 \\
&- \left(x_2^K\right)^2 2(\bar{T}_{he}^R-\bar{T}_{ee}^R)^2 - \left(\tilde{x}_2^K\right)^2 2(\bar{T}_{eh}^R-\bar{T}_{hh}^R)^2 \\
&+ x_1^K\tilde{x}_1^K 4|r_{he}^R r_{hh}^{R*}+r_{ee}^R r_{eh}^{R*}|^2 - x_1^K x_2^K 4|r_{he}^R\bar{t}_{he}^{R*}+r_{ee}^R\bar{t}_{ee}^{R*}|^2 + x_1^K\tilde{x}_2^K 4|r_{he}^R\bar{t}_{hh}^{R*}-r_{ee}^R\bar{t}_{eh}^{R*}|^2 \\
&+ \tilde{x}_1^K x_2^K 4|r_{eh}^R\bar{t}_{ee}^{R*}-r_{hh}^R\bar{t}_{he}^{R*}|^2 - \tilde{x}_1^K\tilde{x}_2^K 4|r_{eh}^R\bar{t}_{eh}^{R*}+r_{hh}^R\bar{t}_{hh}^{R*}|^2 + x_2^K\tilde{x}_2^K 4|\bar{t}_{he}^R\bar{t}_{hh}^{R*}+\bar{t}_{ee}^R\bar{t}_{eh}^{R*}|^2 \,.
\end{aligned}
\tag{63}
$$

The above results are valid for general non-equilibrium distribution. The distribution functions x_i^K and $\tilde{x}_i^K$ can always be expressed as local equilibrium distributions plus 'anomalous' non-equilibrium distributions. Then the purely spectral terms, S^{R-A}, are cancelled exactly by local equilibrium terms in S^K that do not contain a Fermi function.

Equations (51) and (63), combined with Tables (I) for the reflection and transmission probabilities are the central equations needed for calculating the conductance and noise spectrum for NIS junctions with disorder, unconventional pairing and interface screening currents. These formulas are expressed in a form that is closely related to the wave-function-based scattering theory applicable to clean systems. This connection is based on the identification between the scattering amplitudes in the wave function approach and the retarded Ricatti amplitude, γ^R, which, in the clean limit, reduces to the local Andreev reflection amplitude, v/u. However, the Ricatti representation for the propagators is more general, and is capable of incorporating the effects of disorder and inelastic scattering. In our formulation, all observables can then be expressed in terms of the generalized scattering amplitudes collected in Table I, and in the tables in the Appendix. However, the generalized scattering amplitudes are only defined in terms of the quasiclassical Green's functions, through the Ricatti parametrization. We emphasize this fact by keeping the superscript R on all quantities defined in terms of the retarded Green's function.

In summary, to compute the conductance and noise spectrum in voltage-biased NIS junctions we solve the quasiclassical transport equations (5) for $\check{g}$ self-consistently with the gap equations (12), the t-matrix equations (16-17), and the surface coupling to the screening currents, (Eqs. 13-14). We then compute the effective reflection and transmission probabilities, and distribution functions and use Eqs. (51) and (63) to calculate the conductance and the noise spectrum.

III. CONDUCTANCE AND DIFFERENTIAL SHOT NOISE

In the following we use these results to calculate the conductance and noise spectrum for NIS junctions with d-wave superconductors. In the zero-temperature limit, Eq. (51) for the current can be written as

$$
\begin{aligned}
eR_nI(V) = eV + \frac{1}{\mathcal{D}}\int_{-eV}^{0} d\epsilon \,\big\langle v_{fz}\,[\mathcal{R}(\mathbf{p}_f) \\
+\; R_{he}^R(\epsilon,\mathbf{p}_f) - R_{ee}^R(\epsilon,\mathbf{p}_f)]\big\rangle_{\mathbf{p}_f\cdot\hat{z}>0} \,.
\end{aligned}
\tag{64}
$$

The corresponding zero-temperature shot noise, computed at $z=0^-$, from Eqs. (63) and Table (I, takes the form,

$$
\begin{aligned}
R_nS(V) = \frac{2}{\mathcal{D}}\int_{-eV}^{0} d\epsilon \,\big\langle v_{fz}\,\big\{ &R_{ee}^R(\epsilon,\mathbf{p}_f)[1-R_{ee}^R(\epsilon,\mathbf{p}_f)] \\
&+ R_{he}^R(\epsilon,\mathbf{p}_f)[1-R_{he}^R(\epsilon,\mathbf{p}_f)] \\
&+\; 2R_{ee}^R(\epsilon,\mathbf{p}_f)R_{he}^R(\epsilon,\mathbf{p}_f)\big\}\big\rangle_{\mathbf{p}_f\cdot\hat{z}>0} \,.
\end{aligned}
\tag{65}
$$

The normal-state junction resistance is given by $R_n^{-1} = 2\mathcal{A}e^2N_fv_f\mathcal{D}$, where $\mathcal{D}\equiv\langle\cos\theta\mathcal{D}(\mathbf{p}_f)\rangle_{\mathbf{p}_f\cdot\hat{z}>0}$ is the *transport* barrier transparency; $\cos\theta=\hat{p}_f\cdot\hat{z}\geq 0$ is the angle of incidence measured relative to the z-axis. Note that in the normal-state limit for the superconducting electrode, the Andreev reflection probability vanishes, $R_{he}^R(\epsilon,\mathbf{p}_f)\to 0$, the effective $e\to e$ reflection probability reduces to $R_{ee}^R(\epsilon,\mathbf{p}_f)\to\mathcal{R}(\mathbf{p}_f)$, and the integrand of Eq. (64) vanishes. Thus, we recover Ohm's law for the junction I-V characteristic. Similarly, the shot noise in the NIN limit is proportional to $\langle v_{fz}\mathcal{R}(\mathbf{p}_f)\mathcal{D}(\mathbf{p}_f)\rangle_{\mathbf{p}_f}$, which for small transparency corresponds to the Schottky result $S=2eI$. For higher transparency the current noise is reduced compared to the Schottky result.

The above expressions have in the clean limit the same forms as well known scattering theory results.[13,22–24,43–46] Eq. (64) also agrees with calculations of spectral current densities including impurity scattering and subdominant pairing, in Ref. 39.

In the following we present calculations of the zero temperature conductance $\partial I/\partial V$ and differential shot noise, $\partial S/\partial V$, and focus on effects of magnetic fields, impurity scattering, and subdominant pairing. The exact angle dependence of the tunnelling probability is not particularly important for our purposes; so we take it to have the form predicted by an interface δ-function potential,

$$
\mathcal{D}(\mathbf{p}_f) = \mathcal{D}_0\frac{\cos^2\theta}{1-\mathcal{D}_0\sin^2\theta}\,,
\tag{66}
$$

where $\mathcal{D}_0$ is the transparency for normal incidence.

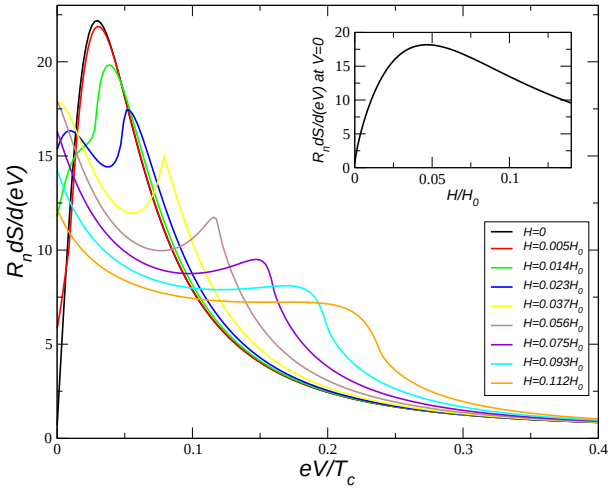

FIG. 3: Zero temperature differential shot noise as a function of voltage in the clean limit for several different external magnetic fields. Inset: The field evolution of the zero-voltage differential shot noise. The transparency of the interface is $\mathcal{D}_0 = 0.1$.

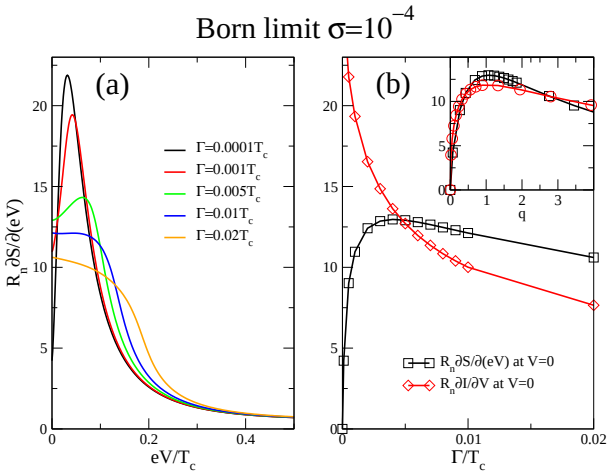

FIG. 4: (a) Differential shot noise for several different pair breaking parameters Γ for scattering in the Born limit ($\sigma = 10^{-4}$). (b) The zero-voltage value of differential shot noise and conductance as a function of Γ. The squares and diamonds are the numerically computed results, while the lines are a guide to the eye. The junction transparency is $\mathcal{D}_0 = 0.1$. In the inset the zero-voltage value of the differential shot noise is plotted as a function of q (c.f. the text), in the Born limit [squares - same data as in the (b)] and unitary limit [circles - same data as in the (b) part of Fig. 5].

A. Pure $d_{x^2-y^2}$-wave: effects of a magnetic field

In zero external magnetic field, the angle resolved differential shot noise is suppressed to zero at zero voltage and has a peak at $\sim \mathcal{D}(\mathbf{p}_f)|\Delta_0(\mathbf{p}_f)|$, where $\Delta_0(\mathbf{p}_f) = \Delta_{B_{1g}}(z \to \infty)\eta_{B_{1g}}(\mathbf{p}_f)$ is the gap in the bulk. This result is due to the resonant enhancement of Andreev reflection by the surface bound state: around the bound state energy ($\epsilon = 0$) within an energy interval set by the bound state width $w_b(\mathbf{p}_f) = a\mathcal{D}(\mathbf{p}_f)|\Delta_0(\mathbf{p}_f)|$, the probability of Andreev reflection is enhanced to unity $R^R_{he}(\epsilon = 0, \mathbf{p}_f) = 1$ independently of the smallness of the transparency and independently of the shape of the order parameter near the junction. The numerical prefactor a is due to the reduction of the bound state width caused by the suppression of the order parameter near the surface. It was computed for small $\mathcal{D}$ in Ref. 47 and can be estimated to be approximately 1/4. As the Andreev reflection probability is enhanced to unity, the normal reflection probability is reduced to zero, $R^R_{ee}(\epsilon = 0, \mathbf{p}_f) = 0$. The result of zero noise at $V = 0$ then follows directly from Eq. (65). The suppression of $\partial S/\partial V$ to zero at zero voltage for zero field is robust under angle integration since the zero-energy bound state is dispersionless. The satellite peak will be located at a voltage of the order $\langle w_b(\mathbf{p}_f)\rangle_{\mathbf{p}_f} \approx \mathcal{D}_0 T_c/2\pi$. This noise-*less* character of the zero-energy bound states in a clean system was recently discussed in Refs. 23,24,46.

In an externally applied magnetic field, the screening currents produce a Doppler shift of the spectrum. The bound state resonance is shifted accordingly. The point of suppressed noise is then shifted to finite voltage and the peak in $\partial S/\partial V$ is pushed to higher voltages linearly with increasing magnetic field. These characteristics of the field evolution of the shot noise spectrum are shown in Fig. 3. The dispersion of the Doppler-shifted ABS leads to non-zero differential shot noise at all voltages. In particular, at zero voltage the differential shot noise develops with increasing magnetic field strength as shown in the inset of Fig. 3.

B. $d_{x^2-y^2}$ pairing with impurity scattering: Andreev vs. tunnel limits

The sensitivity of the noise to changes in the low-energy surface excitation spectrum implies that the results for $S(V)$ in clean d-wave superconductors[23,24,46] are strongly modified by disorder. Here we consider the effects of impurity scattering on the noise spectrum.

In Fig. 4 and Fig. 5 we plot the differential shot noise for several pair breaking parameters, Γ, for scattering in both the Born ($\sigma \ll 1$) and the unitary limits ($\sigma = 1$), respectively. Impurity renormalization leads to broadening of quasiparticle states that depends on the pair breaking parameter, Γ, and the scattering cross section, σ.

The local self energy at the interface is different from that in the bulk because of the formation of surface bound states. In particular, the surface bound state has a large impurity renormalization in the Born limit, but is weakly modified in the unitary limit.[48] This is opposite to the state of affairs in the bulk, where scattering in the unitary limit is more detrimental to the $d_{x^2-y^2}$ order parameter, and produces a low-energy impurity band in the density of states.

Impurity broadening of the surface ABS reduces the

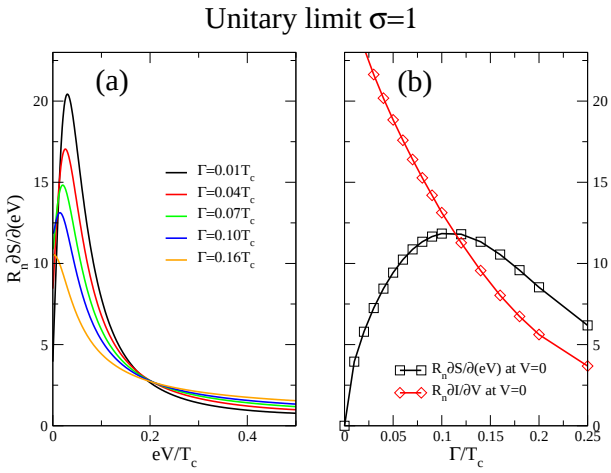

FIG. 5: The same as in Fig. 4 but for scattering in the unitary limit ($\sigma = 1$).

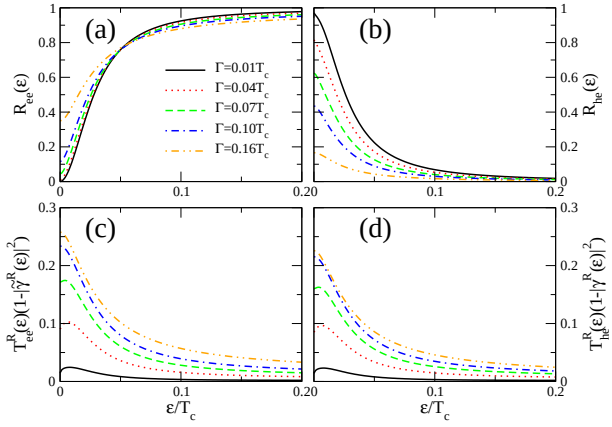

FIG. 6: Scattering probabilities for different pair breaking strengths for tunnelling ranging from the the Andreev limit (black curves) to the tunnel limit (brown curves). The parameters corresponds to unitary scattering in Fig. 5(a), and all probabilities were computed at an incidence angle of 45^o relative to the interface normal. The resonance in the Andreev reflection probability $R_{he}(\epsilon)$ at zero energy (due to the bound state) is broadened by impurity scattered and suppressed in the tunnel limit. The resonance width in the Andreev limit is set by the transparency of the interface. Note that the sum of all probabilities is always equal to one, c.f. Eq. (67).

resonant transmission in the Andreev channel, but opens up the single-particle tunnelling channel. In Fig. 6 we plot the reflection and transmission probabilities for scattering in the unitary limit for several values of the pair breaking parameter. With increasing Γ, the reduction of the Andreev reflection probability R^R_{he} (Fig. 6a) is accompanied by an increase of the normal reflection probability R^R_{ee} (Fig. 6b) and an increase of the transmission probabilities, both transmission without branch conversion $T^R_{ee}(1-|\tilde{\gamma}^R|^2)$ (Fig. 6c) and transmission with branch conversion $T^R_{he}(1-|\gamma^R|^2)$ (Fig. 6d). In particular, the transmission probabilities acquire a resonance form, similar to that in the Andreev reflection channel.

We note that probability is always conserved during scattering at the interface; it can be checked that

$$R^R_{ee} + R^R_{he} + T^R_{ee}(1-|\tilde{\gamma}^R|^2) + T^R_{he}(1-|\gamma^R|^2) = 1. \quad (67)$$

The third and fourth terms, which describe single particle tunnelling, are identically zero in the sub-gap region in the absence of impurity scattering, but become increasingly important as the impurity renormalization increases (see Fig. 6). When the Andreev resonance is reduced and single-particle tunnelling becomes important, the differential shot noise at zero voltage becomes nonzero, as shown in Figs. 4-5. This is in line with the phenomenological discussion in Ref. 46. Thus, we find that the noise-*less* character of the zero-energy surface bound state is quickly lost when intrinsic broadening is present.

To quantitatively assess the importance of impurity scattering in tunnelling, the contribution to the width of the bound state from impurity broadening, which we denote w_i, has to be compared with the contribution set by the transparency of the interface, w_b, introduced in the previous section. The width w_i is related to the imaginary part of the impurity self energy Σ^R_3 near the surface. Unfortunately, a rigorous analytic calculation of w_i in which the spatial dependence of the impurity self energy and the order parameter are taken into account has so far not been carried out (see, however, the scaling analysis in Ref. 48). We estimate the width to be $w_i = c|\mathrm{Im}\{\Sigma^R_3(\epsilon=0, z=0^+)\}|$, where c is numerical factor which corrects for the spatial dependence of the self energies. In the limit $w_i \gg w_b$, which we call the 'tunnel limit', intrinsic broadening is large and only single-particle tunnelling is important. Andreev reflection can then be neglected and the shot noise for low transparency reduces to the Schottky form $S = 2eI$, and does not contain any new information that can not be extracted from the current. On the other hand, in the limit $w_i \ll w_b$, which we call the 'Andreev limit', impurity broadening is negligible, single particle tunnelling is suppressed and Andreev reflection is resonant. In this limit the shot noise is non-trivial. In Figs. 4-5, the crossover between these two regimes is displayed for impurity scattering in the Born and unitary limits. It is clear that the impurity renormalization near the surface is much larger in the Born limit compared to the unitary limit: the crossover appears for $\Gamma/T_c \sim 10^{-3}$ in the Born limit, which is two orders of magnitudes smaller than in the unitary limit. However, if we plot $R_n\partial S/\partial(eV)$ at $V=0$ as a function of $q = w_i/\langle w_b(\mathbf{p}_f)\rangle_{\mathbf{p}_f}$, with the numerically computed $\mathrm{Im}\{\Sigma^R_3(\epsilon=0, z=0^+)$ and an estimate $c = 1/3$ in the Born limit and $c = 3$ in the unitary limit, we find that the crossover appears near $q \sim 1$ in both limits, see inset of Fig. 4(b).

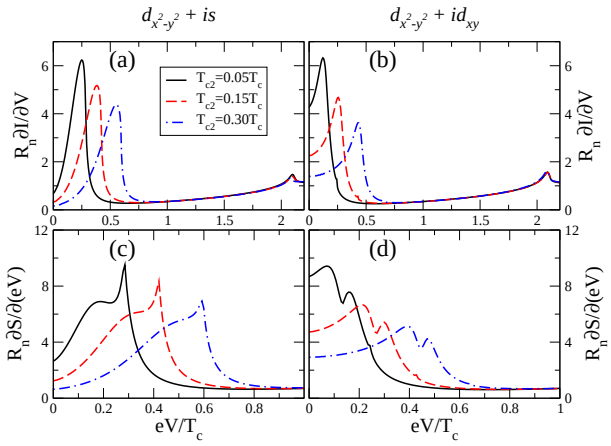

FIG. 7: (a)-(b) Conductance and (c)-(d) differential shot noise for an order parameter with an s subdominant component (left column) and a d_{xy} subdominant component (right column) for several different interaction strengths. The barrier transparency is $\mathcal{D}_0 = 0.1$, and the system is in the Andreev limit ($\Gamma = 0.001T_c$, $\sigma = 10^{-4}$).

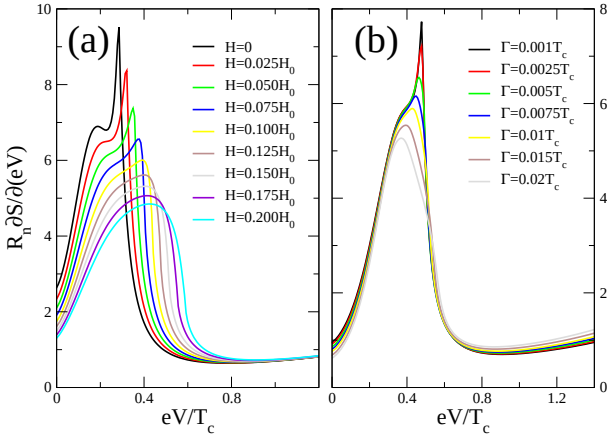

FIG. 8: (a) Magnetic field dependence of differential shot noise for a $d_{x^2-y^2} + is$ order parameter with $T_{c2} = 0.05T_c$. Here is $\Gamma = 0.001T_c$ and $\sigma = 10^{-4}$. (b) Differential shot noise as a function of pair breaking parameter Γ in the Born limit ($\sigma = 10^{-4}$). Here is $T_{c2} = 0.2T_c$. In both cases is $\mathcal{D}_0 = 0.1$.

C. $d_{x^2-y^2} + is$ and $d_{x^2-y^2} + id_{xy}$ symmetries

Finally, we consider the signatures of a surface phase transition from an inhomogeneous $d_{x^2-y^2}$ surface phase, to a surface state with mixed symmetry: $d_{x^2-y^2} + is$ or $d_{x^2-y^2} + id_{xy}$. In the clean limit the noise spectrum is sensitive to the change the surface excitation spectrum induced by the sub-dominant pairing channel. When a complex order parameter develops near the surface, time-reversed partners of the two-fold degenerate zero-energy bound states are shifted in opposite directions from the Fermi level. The positive energy bound state spectra for these mixed-symmetry phases are shown in Fig. (1). A surface current, and an associated spontaneous magnetic field, are generated. This symmetry breaking can be detected in the conductance as a spontaneous splitting of the zero-bias conductance peak, or as a spontaneous magnetic signal from the surface.

In the shot noise, for a clean system, we thus expect the point of vanishing noise to disperse with angle of incidence, in a similar way the Doppler shift changes the shot noise spectrum in an applied field. In addition to the dispersion of the bound states with angle, there is an additional mechanism of dispersion due to electron-hole de-phasing, which appears at non-zero energies when the order parameter has a spatial dependence (pairbreaking suppression near the surface). These mechanisms of dispersion of the bound state conspire to wash out much of the structure one might otherwise expect to observe in the shot noise near zero voltage. Nevertheless, for a clean superconductor, a characteristic differences can be seen in $\partial S/\partial V$ for the cases of sub-dominant s- and d_{xy} order parameters.

In Fig. 7 we plot the conductance and differential shot noise for several different interaction strengths, in both the s and d_{xy} sub-dominant channels. There is not difference in the signatures of the two different subdominant components in the conductance: in both the s and d_{xy} cases the zero-bias conductance peak is split and appears at a finite voltage related to the size of the subdominant order parameter. On the other hand, in the shot noise, there is a double peak structure in both cases, with the high-voltage peak bigger than the low-voltage peak for the s-wave case, but with a reversal in spectral weight between low- and high-voltage peaks for the d_{xy} case. This reversal reflects the difference in the dispersion of the the bound states for the two different pairing channels, which affects the point of suppressed shot noise (as well as the associated peak in $\partial S/\partial V$). The shift to finite voltage is larger and disperses less in the s-wave case, compared to the d_{xy} case.

Application of a magnetic field introduces additional dispersion, and the angle integration leads to a reduction of the structures. For both types of order parameters, the double peak evolves with increasing magnetic field strength into a single peak on a scale H/H_0 set by the size of the subdominant gap, see Fig. 8(a).

As in the pure d-wave case discussed in the previous section, impurity scattering broaden the bound state resonance and reduces the structure in the shot noise. Thus, with increasing pair breaking parameter the two peaks in the shot noise merge into a single peak and, in the tunnel limit, the differential shot noise reduces to the conductance, see Fig. 8(b).

IV. DISCUSSION AND SUMMARY

In conclusion, shot noise can be a useful tool to extract detailed information about properties of junctions between normal metals and unconventional superconduc-

tors. However, a necessary condition is that the system is in the Andreev limit, $w_i \ll w_b$, as shown in Figs. 4-6. This is a rather restrictive condition at present, since in most experiments the zero-bias conductance peak is broadened by disorder, see however Ref. 49.

In several recent experiments[3–5] the density of states around single impurities or inhomogeneities were mapped out by c-axis STM spectroscopy. The results are discussed in terms of low energy states bound to a single impurity scattering in the unitary limit, in line with theoretical works in Refs. 50–52. Thus, if impurities in the high-T_c superconductors are indeed scattering in the unitary limit, we expect that the surface bound states will not be particularly broadened, and tunnelling in the Andreev limit should be possible to achieve experimentally in a clean sample. The mean free path corresponding to $q \ll 1$ in the unitary limit (for the parameters in Fig. 5) is estimated to be of the order of tenths of coherence lengths, which is achievable experimentally.

There are other sources of broadening of the surface/interface bound states that were not considered in this paper. In particular, it is clear that surface roughness will drive the system towards the tunnel limit, because non-specular scattering of quasiparticles to the nodes of the order parameter broadens the bound states just as impurity scattering does. Therefore, to extract information from shot noise it will be important to have a specularly reflecting junction, or tunnel from an STM tip directly into the ab-plane of a specular portion of a superconductor surface.

Under these circumstances, information about the superconductor properties can be deduced via the particular properties of the zero energy surface bound states. The shot noise in a purely $d_{x^2-y^2}$-wave superconductor is suppressed around low voltage and approaches zero in the clean limit. The characteristic magnetic field dependence shown in Fig. 3 can then be used to test the theory. The zero-voltage shot noise level changes according to the inset of Fig. 3, and the satellite peak is linearly pushed out with increasing magnetic field strength. The double peak structure shown in Fig. 7 serves as a fingerprint of the symmetry of the subdominant pairing channel.

Acknowledgments

We thank A. Vorontsov and M. Eschrig for valuable discussions. This work was supported by the NSF, grant DMR 9972087, the Swedish Research Council, VR, and STINT, The Swedish Foundation for International Cooperation in Research and Higher Education.

Appendix

In this appendix we tabulate the Andreev reflection probabilities expressed in terms of the barrier reflection and transmission probabilities and coherence amplitudes for incoming trajectories in Table II, and in Table III we summarize the transmission and reflection probabilities that enter the boundary conditions for the distribution functions in Eqs. (33-36).

* Electronic address: sauls@northwestern.edu

[1] C. C. Tsuei and J. R. Kirtley, Rev. Mod. Phys. **72**, 969 (2000).
[2] D. VanHarlingen, Rev. Mod. Phys. **67**, 515 (1995).
[3] E. W. Hudson, S. H. Pan, A. K. Gupta, K.-W. Ng, and J. C. Davis, Science **285**, 88 (1999).
[4] A. Yazdani, C. M. Howald, C. P. Lutz, A. Kapitulnik, and D. M. Eigler, Phys. Rev. Lett. **83**, 176 (1999).
[5] S. H. Pan, E. W. Hudson, K. M. Lang, H. Eisaki, S. Uchida, and J. C. Davis, Nature **403**, 746 (2000).
[6] M. Covington, M. Aprili, E. Paraoanu, L. H. Greene, F. Xu, J.Zhu, and C. A. Mirkin, Phys. Rev. Lett. **79**, 277 (1997).
[7] J. Geerk, X. X. Xi, and G. Linker, Zeit.f. Physik **73**, 329 (1988).
[8] J. Lesueur, L. H. Greene, W. L. Feldman, and A. Inam, Physica C **191**, 325 (1992).
[9] M. Fogelström, D. Rainer, and J. A. Sauls, Phys. Rev. Lett. **79**, 281 (1997).
[10] M. Fogelström and D. Rainer and J. A. Sauls, Cond-Mat **0302197**, 4 (2003).
[11] A. Poenicke, M. Fogelström, and J. A. Sauls, Physica **B 284-288**, 589 (2000), proceedings of LT22.
[12] L. Buchholtz, M. Palumbo, D. Rainer, and J. A. Sauls, J. Low Temp. Phys. **101**, 1099 (1995), [http://xxx.lanl.gov/abs/cond-mat/9511028].
[13] Y. Tanaka and S. Kashiwaya, Phys. Rev. Lett. **74**, 3451 (1995).
[14] C. R. Hu, Phys. Rev. Lett. **72**, 1526 (1994).
[15] V. A. Khlus, Sov. Phys. JETP **66**, 1243 (1987).
[16] M. Graf, A. Balatsky, and J. Sauls, Phys. Rev. **B61**, 3255 (2000), [http://xxx.lanl.gov/abs/cond-mat/9907300].
[17] M. Matsumoto and H. Shiba, J. Phys. Soc. Jpn. **65**, 2194 (1996).
[18] M. Sigrist, D. Bailey, and R. Laughlin, Phys. Rev. Lett. **74**, 3249 (1995).
[19] L. Buchholtz, M. Palumbo, D. Rainer, and J. A. Sauls, J. Low Temp. Phys. **101**, 1079 (1995), [http://xxx.lanl.gov/abs/cond-mat/9511027].
[20] R. Krupke and G. Deuthuscher, Phys. Rev. Lett. **83**, 4634 (2001).
[21] W. K. Neils and D. J. Van Harlingen, Phys. Rev. Lett. **88**, 047001 (2002).
[22] Y. M. Blanter and M. Büttiker, Phys. Rep. **336**, 1 (2000).
[23] J.-X. Zhu and C. S. Ting, Phys. Rev. B **59**, R14165 (1999).
[24] Y. Tanaka, T. Asai, N. Yoshida, J. Inoue, and S. Kashi-

TABLE II: The Andreev reflection probabilities. The denominators are listed in Table III.

$r_{he} = \tilde{\Gamma}_1^R = [R(1+\tilde{\gamma}_2^R\gamma_2^R)\tilde{\gamma}_1^R + D(1+\tilde{\gamma}_1^R\gamma_2^R)\tilde{\gamma}_2^R]/\zeta_1$
$r_{eh} = \Gamma_1^R = [R(1+\gamma_2^R\tilde{\gamma}_2^R)\gamma_1^R + D(1+\gamma_1^R\tilde{\gamma}_2^R)\gamma_2^R]/\zeta_2$
$\bar{r}_{he} = \tilde{\Gamma}_2^R = [R(1+\gamma_1^R\tilde{\gamma}_1^R)\tilde{\gamma}_2^R + D(1+\tilde{\gamma}_2^R\gamma_1^R)\tilde{\gamma}_1^R]/\zeta_3$
$\bar{r}_{eh} = \Gamma_2^R = [R(1+\gamma_1^R\tilde{\gamma}_1^R)\gamma_2^R + D(1+\gamma_2^R\tilde{\gamma}_1^R)\gamma_1^R]/\zeta_4$

TABLE III: Scattering probabilities for x^K distribution functions in the stationary SIS junction setup.

$\bar{T}_{hh} = D\lvert 1+\tilde{\gamma}_1^R\gamma_2^R\rvert^2/\lvert\zeta_1\rvert^2$	$\bar{T}_{he} = RD\lvert\tilde{\gamma}_1^R - \tilde{\gamma}_2^R\rvert^2/\lvert\zeta_1\rvert^2$	$R_{hh} = R\lvert 1+\tilde{\gamma}_2^R\gamma_2^R\rvert^2/\lvert\zeta_1\rvert^2$	$\zeta_1 = 1 + R\gamma_2^R\tilde{\gamma}_2^R + D\tilde{\gamma}_1^R\gamma_2^R$
$\bar{T}_{ee} = D\lvert 1+\gamma_1^R\tilde{\gamma}_2^R\rvert^2/\lvert\zeta_2\rvert^2$	$\bar{T}_{eh} = RD\lvert\gamma_1^R - \gamma_2^R\rvert^2/\lvert\zeta_2\rvert^2$	$R_{ee} = R\lvert 1+\gamma_2^R\tilde{\gamma}_2^R\rvert^2/\lvert\zeta_2\rvert^2$	$\zeta_2 = 1 + R\gamma_2^R\tilde{\gamma}_2^R + D\gamma_1^R\tilde{\gamma}_2^R$
$T_{hh} = D\lvert 1+\tilde{\gamma}_2^R\gamma_1^R\rvert^2/\lvert\zeta_3\rvert^2$	$T_{he} = RD\lvert\tilde{\gamma}_2^R - \tilde{\gamma}_1^R\rvert^2/\lvert\zeta_3\rvert^2$	$\bar{R}_{hh} = R\lvert 1+\gamma_1^R\tilde{\gamma}_1^R\rvert^2/\lvert\zeta_3\rvert^2$	$\zeta_3 = 1 + R\gamma_1^R\tilde{\gamma}_1^R + D\tilde{\gamma}_2^R\gamma_1^R$
$T_{ee} = D\lvert 1+\gamma_2^R\tilde{\gamma}_1^R\rvert^2/\lvert\zeta_4\rvert^2$	$T_{eh} = RD\lvert\gamma_2^R - \gamma_1^R\rvert^2/\lvert\zeta_4\rvert^2$	$\bar{R}_{ee} = R\lvert 1+\gamma_1^R\tilde{\gamma}_1^R\rvert^2/\lvert\zeta_4\rvert^2$	$\zeta_4 = 1 + R\gamma_1^R\tilde{\gamma}_1^R + D\gamma_2^R\tilde{\gamma}_1^R$

waya, Phys. Rev. B **61**, R11902 (2000).

[25] J. C. Cuevas and M. Fogelström, Phys. Rev. B **64**, 104502 (2001).

[26] J. C. Cuevas and M. Fogelström, Phys. Rev. Lett. **89**, 227003 (2002).

[27] J. W. Serene and D. Rainer, Phys. Rep. **101**, 221 (1983).

[28] D. N. Langenberg and A. I. Larkin, *Nonequilibrium Superconductivity, Modern Problems in Condensed Matter Physics*, vol. 12 (North Holland, Amsterdam, 1986).

[29] G. Eilenberger, Zeit.f. Physik **214**, 195 (1968).

[30] A. I. Larkin and Y. N. Ovchinnikov, Sov. Phys. JETP **28**, 1200 (1969).

[31] M. Matsumoto and H. Shiba, J. Phys. Soc. Jpn. **64**, 1703 (1995).

[32] M. Aprili, E. Badica, and L. H. Greene, Phys. Rev. Lett. **83**, 4630 (1999).

[33] M. J. Graf, S.-K. Yip, J. A. Sauls, and D. Rainer, Phys. Rev. B **53**, 15147 (1996), [http://xxx.lanl.gov/abs/cond-mat/9509046].

[34] A. V. Zaĭtsev, Sov. Phys. JETP **59**, 1015 (1984).

[35] A. Millis, D. Rainer, and J. A. Sauls, Phys. Rev. **B38**, 4504 (1988).

[36] A. Shelankov, J. Low Temp. Phys. **60**, 29 (1985).

[37] V. A. Khlus, Sov. Phys. JETP **66**, 1243 (1988).

[38] G. Kieselmann, Phys. Rev. B **35**, 6762 (1987).

[39] M. Eschrig, Phys. Rev. B **61**, 9061 (2000).

[40] Y. Nagato, K. Nagai, and J. Hara, J. Low Temp. Phys. **93**, 33 (1993).

[41] M. Eschrig, J. A. Sauls, and D. Rainer, Phys. Rev. B **60**, 10447 (1999), [http://xxx.lanl.gov/abs/cond-mat/9805299].

[42] N. Schopohl and K. Maki, Physica **B 204**, 214 (1995).

[43] G. E. Blonder, M. Tinkham, and T. M. Klapwidjk, Phys. Rev. B **25**, 4515 (1982).

[44] M. P. Anantram and S. Datta, Phys. Rev. B **53**, 16390 (1996).

[45] J. P. Hessling, V. S. Shumeiko, Y. M. Galperin, and G. Wendin, Europhys. Lett. **34**, 49 (1996).

[46] T. Löfwander, V. S. Shumeiko, and G. Wendin, Physica C **367**, 86 (2002).

[47] Y. S. Barash, Phys. Rev. B **61**, 678 (2000).

[48] A. Poenicke, Y. S. Barash, C. Bruder, and V. Istyukov, Phys. Rev. B **59**, 7102 (1999).

[49] J. Y. T. Wei, N.-C. Yeh, D. F. Garrigus, and M. Strasik, Phys. Rev. Lett. **81**, 2542 (1998).

[50] P. A. Lee, Phys. Rev. Lett. **71**, 1887 (1993).

[51] M. I. Salkola, A. V. Balatsky, and D. J. Scalapino, Phys. Rev. Lett. **77**, 1841 (1996).

[52] M. E. Flatté and J. M. Byers, Phys. Rev. Lett. **80**, 4546 (1998).

[53] We use the simplest polynomials to represent the basis functions. The true basis functions are obtained as eigenfunctions of the linearized gap equation with true pairing interaction, and in general differ from the polynomial functions we use here.

[54] The phases of r and d does not play a role in our calculations and can be eliminated; thus, both r and d are taken to be real.